(Preprint) AAS 20-436

LOW-THRUST TRANSFER TO INTERPLANETARY TRAJECTORIES FROM LUNAR TRAJECTORIES WITH RIDESHARE

Darcey R. Graham[*], Jacob A. Englander[†], Nicholas J. Rattenbury[‡] and John E. Cater[§]

Accessing interplanetary space is challenging when using low thrust systems. Injecting spacecraft onto interplanetary trajectories is difficult with small launch vehicles, but it is possible to instead transfer to an interplanetary trajectory from a lunar flyby. Such cases are useful, for example, in rideshares between lunar and interplanetary missions. This work examines the problem of rideshare for small satellites onto lunar flyby trajectories, with transfers to an interplanetary trajectory. Low thrust interplanetary trajectories are examined starting from a rideshare mission on a lunar trajectory using delivery systems based on a modified Rocket Lab USA Electron vehicle and Photon stage.

INTRODUCTION

The preliminary design of low-thrust trajectories poses a complex problem; there are many often non-intuitive variables to decide, such as the control vector determining the direction and magnitude of thrusting, and a large design space must be searched. Complexity also arises from the continuous nature of many low-thrust systems. High-thrust systems can produce the necessary velocity change for a manoeuvre in a space of time short enough to be considered instantaneous. Low-thrust systems such as electric propulsion must thrust for hours or days, so cannot be discretised in this way. Preliminary designers must search a large space for feasible solutions to a problem. These low-fidelity solutions are fed as an initial guess into higher-fidelity models capable only of searching a much smaller problem space.

Many methods for preliminary trajectory design exist, making use of direct or indirect optimisation techniques. Indirect methods[1,2] solve the dual problem for the state and co-state vectors. This tends to give a more accurate solution than direct methods, but requires a better initial guess, including for the non-intuitive co-state vectors. Direct methods[3–5] typically convert the problem into a non-linear programming (NLP) problem which can be solved using an NLP solver such as SNOPT.[6] Shape-based methods[7–9] are useful in eliminating the need to guess non-intuitive variables by assuming, and describing analytically, the shape of the trajectory instead of searching for a thrust profile. However, these methods lack flexibility and may call for infeasibly high thrust.

[*]PhD Student, Department of Physics, University of Auckland, Private Bag 92019, Auckland, New Zealand
[†]Aerospace Engineer, NASA Goddard Space Flight Center, Navigation and Mission Design Branch, 8800 Greenbelt Rd, Greenbelt, MD 20771, Member AAS
[‡]Department of Physics, University of Auckland, Private Bag 92019, Auckland, New Zealand
[§]Department of Engineering Science, University of Auckland, Private Bag 92019, Auckland, New Zealand

This study uses the Sims-Flanagan transcription[10] to discretise a continuous low-thrust trajectory into a series of time steps. For each time step the thrust and perturbations are approximated as an instantaneous impulse at its centre. This removes thrust and perturbations from the equations of motion, simplifying their integration for optimisation. Here the NLP problem is solved by *fmincon* in Matlab. The solution uses a monotonic basin hopping (MBH) algorithm[11–13] which searches for local minima before jumping to a new point in the problem space. This allows a global search to be conducted and enables feasible solutions to be found with little input from a mission designer.

Following the success of NASA's MarCO mission[14] demonstrating the interplanetary capabilities of CubeSats, interest has been sparked in exploring the possibilities of small satellite missions. Smaller satellites are cheaper to produce and launch, and with the development of features such as Rocket Lab's Maxwell CubeSat Dispenser, the ease of integration is growing. The goal of this work was to develop a model capable of finding low-thrust Earth-Venus trajectories starting from a rideshare mission injecting into a non-escape trajectory from a Rocket Lab Electron vehicle and Photon stage.

However, small satellites are unlikely to be given their own dedicated launch, posing an additional challenge to interplanetary mission designers. On the rideshare mission considered here, a small satellite does not have a launch injection into an interplanetary trajectory as assumed by many previous models. This study applies a multiple gravity-assist low-thrust (MGALT) method[15–17] to the problem of escape from the Earth-Moon system starting on a lunar trajectory on a rideshare mission. The resulting escape is patched to an Earth-Venus trajectory. Third-body perturbations are included. The model developed in this study is capable of finding Earth-Venus trajectories from launch with very little input from the mission designer.

MULTIPLE GRAVITY-ASSIST LOW-THRUST (MGALT) MODEL

The MGALT model used in this study is based on the Sims-Flanagan transcription[10] combined with a two-body patched conic model. The effect of the gravitational force of additional bodies are included as perturbations. The Sims-Flanagan transcription divides the trajectory into phases, which each start and end at a control point. Control points can be planets, asteroids, or free bodies in space, and can be selected by an outer loop optimiser or the mission designer. The control points in the Earth-Moon escape portion of this trajectory are: launch from Earth, the first and second lunar gravity assists, and escape at the edge of the Earth's sphere of influence. For the trip to Venus, which consists of one phase, the control points are simply the Earth escape previously determined, and arrival at Venus.

This is a forwards-backwards shooting method, meaning the phase is split into two halves. The first half is propagated forwards in time from the earlier control point. The second half is propagated backwards in time from the later control point. Each half of the phase ends in a match point at which nonlinear constraints drive the forwards- and backwards-shooting arcs to meet.

Each phase is further divided into N segments of equal time as shown in Figure 1. The continuous thrusting of the spacecraft, as well as third body perturbations, are approximated as an instantaneous change in velocity and mass at the centre of each segment. An n-body Sims-Flanagan transcription such as this has been applied previously to the Jupiter system.[18] In between these impulses, the state vector of the spacecraft is propagated using Kepler's equation.[19] The propagator used in this study uses universal variables[20] and the Laguerre-Conway root-finding method,[21] as this rapidly converges to a solution from a very poor initial guess.[21,22]

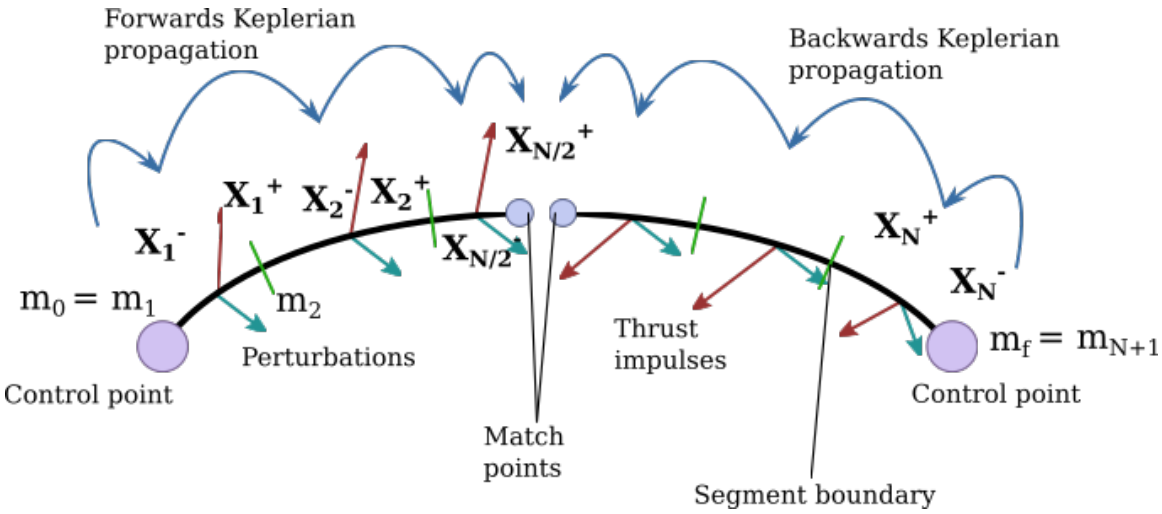

Figure 1. A single MGALT phase showing division into N segments with impulses at their centre. $\mathbf{X}_k^{\pm}$ indicates the state vector before (-) and after (+) each impulse, and m indicates spacecraft mass.

The change in velocity at the centre of each segment is determined by Equation 1:

$$\begin{aligned} \mathbf{v}_k^+ &= \mathbf{v}_k^- + \Delta v_{\max_k} \mathbf{u}_k + \sum_{p=1}^{n} -\frac{\mu_p}{r_p^3} \mathbf{r}_p \Delta t_k \quad \text{forwards shooting} \\ \mathbf{v}_k^- &= \mathbf{v}_k^+ - \Delta v_{\max_k} \mathbf{u}_k - \sum_{p=1}^{n} -\frac{\mu_p}{r_p^3} \mathbf{r}_p \Delta t_k \quad \text{backwards shooting,} \end{aligned} \tag{1}$$

where k indicates the index of the time step, a superscript $+$ indicates the state immediately after the impulse, a superscript $-$ the state immediately prior to the impulse, $\mathbf{v}$ is the velocity vector of the spacecraft, Δv_{max_k} is the maximum change in velocity which can be achieved by the thrusters over the entire segment as calculated in Equation 3, μ_p is the gravitational parameter of an additional body acting to perturb motion, $\mathbf{r}_p$ is the distance between the spacecraft and that body, Δt_k is the time over which the segment takes place, and $\mathbf{u}_k$ is the control vector.

In Equation 1, the first term is the velocity just before the impulse, the second term is the change in velocity due to thrusting, and the third term is the change in velocity due to perturbing bodies. Ephemeris data on the perturbing bodies is provided by SPICE.[23,24] In the model presented here, the two-body system in the Earth-escape leg of the journey has the Earth as its central body with the Moon as a perturbing body. In the interplanetary portion of the journey, the Sun is the central body, and the Earth and target planet (in this case, Venus) are perturbing bodies. The control vector is a decision variable controlling the thrusting of the spacecraft with magnitude constrained to be less than unity:

$$||\mathbf{u}_k|| = \sqrt{u_{x_k}^2 + u_{y_k}^2 + u_{z_k}^2} \leq 1, \tag{2}$$

which is the first constraint enforced by the optimiser. The maximum possible change in velocity is

$$\Delta v_{\max_k} = \frac{N_{\text{active}} D T_{\max} \Delta t_k}{m_k}, \tag{3}$$

where N_{active} is the number of active thrusters, D is the thruster duty cycle, $T_{\max}$ is the maximum thrust for the segment, and m_k is the mass at the impulse.

The change in mass is instantaneous though not affected by third-body perturbations as using fuel to fire thrusters is the only cause of changes in mass. The instantaneous change in mass at the centre of each segment is

$$m_k = \begin{cases} m_{k-1} - ||\mathbf{u}_{k-1}|| D \Delta t_k \dot{m}_{\max_k} & \text{forward propagation} \\ m_{k+1} + ||\mathbf{u}_k|| D \Delta t_k \dot{m}_{\max_k} & \text{backward propagation,} \end{cases} \tag{4}$$

where mass flow rate is

$$\dot{m}_{\max_k} = \frac{T_{\max}}{I_{\text{sp}} g_0}, \tag{5}$$

I_{sp} is the specific impulse, and g_0 is the gravitational acceleration at the surface of the Earth. A constant $T_{\max}$ is assumed, which in reality will change throughout the flight. MGALT models exist which also include a power model, where power to the thrusters depends on proximity to the Sun and the power useage of the spacecraft bus.[25,26] As more power will be available as the spacecraft grows closer to the Sun (and so to Venus), this is less important for the level of fidelity considered here but could be included in future work.

Table 1. Decision variables for the Earth-Moon escape portion of the trajectory.

Variable	Description	Number
t_0	Launch epoch	1
v_∞	Launch impulse magnitude	1
C3	Initial characteristic energy	1
ω	Argument of perigee of initial orbit	1
e	Eccentricity of initial orbit	1
i	Inclination of initial orbit	1
Ω	Right ascension of ascending node of initial orbit	1
ν	True anomaly of initial orbit	1
Δt_p	Time of flight of phase	N_p
$\mathbf{v}_{\infty_i}$	Excess velocity vector prior to gravity assist	$3(N_p - 1)$
$\mathbf{v}_{\infty_f}$	Excess velocity vector immediately after gravity assist	$3(N_p - 1)$
$\mathbf{v}_f$	Velocity vector at escape from Earth-Moon system	3
m_f	Final phase mass	N_p
$\mathbf{r}_f$	Point of escape on edge of Earth sphere of influence in Cartesian coordinates	3
$\mathbf{u}$	Control vector	$3N$

The decision variables in describing an Earth-escape trajectory and interplanetary trajectory are shown respectively in Tables 1 and 2, where N_p is the number of phases and N is the number of segments in each phase. To complete the characterisation of the NLP optimisation problem to be solved, the remaining constraints to be defined are the match point constraints, time constraints and gravity assist constraints. As previously stated, the MGALT model uses forwards-backwards

Table 2. Decision variables for the interplanetary portion of the trajectory.

Variable	Description	Number
t_0	Launch epoch	1
$\mathbf{v}_i$	Excess velocity at Earth escape	3
$\mathbf{v}_f$	Excess velocity on arrival at Venus	3
Δt_p	Time of flight of phase	N_p
$\mathbf{v}_{\infty_i}$	Excess velocity vector prior to gravity assist	$3(N_p-1)$
$\mathbf{v}_{\infty_f}$	Excess velocity vector immediately after gravity assist	$3(N_p-1)$
m_i	Initial mass at Earth escape	1
m_f	Final phase mass	N_p
$\mathbf{u}$	Control vector	$3N$

shooting with a central match point constrained to be continuous. This is done by imposing the match point constraint on the state vector:

$$\mathbf{c} = \mathbf{X}_B - \mathbf{X}_F = \begin{bmatrix} \mathbf{r}_B - \mathbf{r}_F \\ \mathbf{v}_B - \mathbf{v}_F \\ m_B - m_F \end{bmatrix} = \mathbf{0}, \tag{6}$$

where $\mathbf{X}_B$ and $\mathbf{X}_F$ are state vectors at the match point of the backwards and forwards propagated arcs, respectively. The time of flight must also be constrained so that the sum of the time of flights of each phase does not exceed the total time of flight. The constraint to achieve this is

$$c_{\text{TOF}} = \sum_{i=1}^{N_p} \Delta t_{p_i} \leq \Delta t_{\max}. \tag{7}$$

Gravity Assists

Gravity assists are modelled using a patched conic approximation with a zero radius sphere of influence. The change in velocity is modelled by selecting the velocity before and after the gravity assist manoeuvre as decision variables, with nonlinear constraints ensuring the manoeuvre is physically realisable. Although the velocity magnitude relative to the central body may increase, the magnitude of the velocities relative to the flyby body (in the escape portion, the Moon) must be equal to satisfy conservation of momentum. This provides the constraint function:

$$c_{v_\infty} = v_{\infty_f} - v_{\infty_i} = 0, \tag{8}$$

where v_{∞_f} is excess velocity immediately after and v_{∞_i} is excess velocity immediately before a gravity assist manoeuvre.

The other important condition is that the spacecraft must not pass lower than a specified safe distance h_{safe} above the flyby target. This second nonlinear constraint on gravity assist manoeuvres occurs at the end of each phase and also ensures the turn angle of the flyby is feasible:

$$
\begin{aligned}
c_{\text{altitude}} &= r_{\text{periapse}} \geq r_{\text{body}} + h_{\text{safe}} \\
&= \frac{\mu}{v_\infty^2}\left(\frac{1}{\sin\left(\frac{\delta}{2}\right)} - 1\right) - r_{\text{body}} - h_{\text{safe}} \geq 0,
\end{aligned} \tag{9}
$$

where r_{periapse} is the closest approach of the flyby to the centre of the target, r_{body} is the radius of the target, and

$$
\delta = \arccos\left(\frac{\mathbf{v}_{\infty_i}\mathbf{v}_{\infty_f}}{v_{\infty_i}v_{\infty_f}}\right). \tag{10}
$$

OPTIMISATION WITH MONOTONIC BASIN HOPPING (MBH)

The problem is cast as an NLP problem and solved by MATLAB's *fmincon* function. The initial guess for each of the decision variables is chosen randomly by the model within bounds specified by the designer. This enables a wide parameter space to be explored with little prior knowledge of the solution, permitting the discovery of trajectories which may not otherwise have been apparent. The gradients are determined by finite differences. Upper and lower bounds can be specified or a decision variable can be forced by a mission designer is desired to guide a search or help meet a requirement. However, it has been shown that providing analytical gradients to the optimiser significantly increases the likelihood of convergence to a feasible solution.[25] A further issue is that *fmincon* cannot take advantage of the sparsity pattern of the problem Jacobian.[27] Using a solver which can, such as SNOPT,[6] would significantly decrease run time.

In order to search a wide global problem space based on one very poor initial guess, an MBH algorithm is utilised.[11,12,22] MBH searches in the local region of an initial guess by repeating solves of the NLP problem, then after a meeting the stop condition or after finding a local minimum, jumps to a new initial guess for its search. The algorithm stores the results to an archive and selects the best possible one; that is, the one which minimises the cost function (in this case, the cost function maximises final mass), while satisfying the nonlinear constraints.

ESCAPING THE EARTH-MOON SYSTEM

The Earth-Moon escape trajectory is split into three phases: a thrust arc from launch to the first lunar gravity assist; a second thrust arc between the first and second lunar gravity assist manoeuvres; and a coast from the second lunar gravity assist to escape at the edge of the Earth's sphere of influence, considered here to be 1.47x10^{6}km. The spacecraft is considered to have escaped the Earth-Moon system when it reaches the edge of the sphere of influence.

The spacecraft begins from a launch achievable by an Electron launch vehicle, in this case assuming a launch C3 of -2km^2/s^2 and mass of 10.5kg. The thruster onboard the small satellite is assumed to have a constant thrust of 0.9mN when firing, and a specific impulse of 1800s. Each of the three phases are split into 40 segments. The model generates a random initial guess, then MBH finds a minimum with an objective function maximising final mass. The decision variables for this trajectory are shown in Table 1. For the results presented here, lower bounds were placed on the eccentricity to be greater than 0.967, as this permits the initial orbit to reach the Moon while also starting a safe distance above the Earth. True anomaly was set to 0 to force the trajectory to start

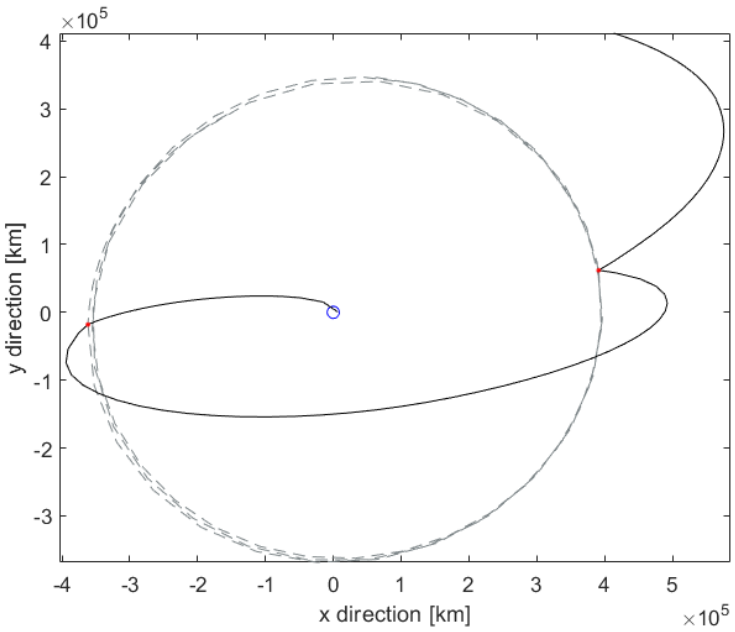

Figure 2. An example Earth escape trajectory generated using the method described here. The Earth is at the origin, the Moon's orbit the grey dashed line, spacecraft trajectory the solid black line, and lunar gravitational assists are red dots.

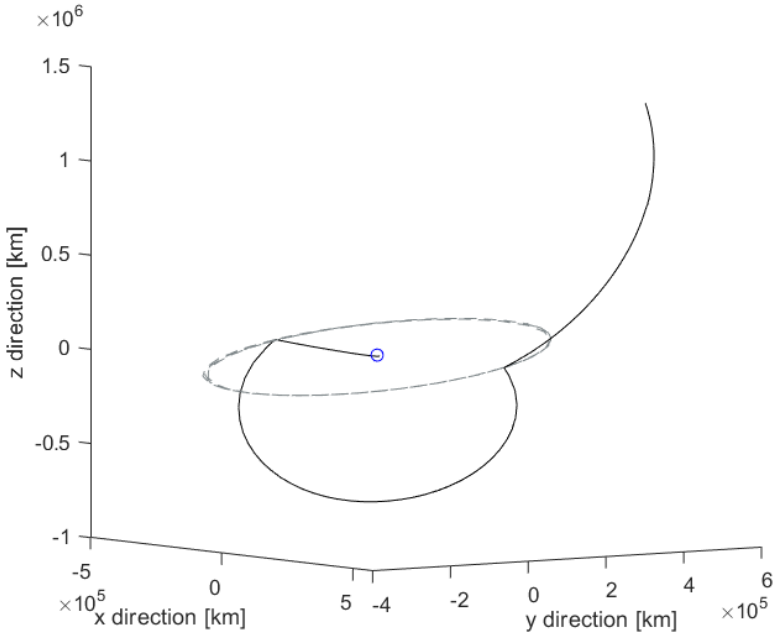

Figure 3. A different view of the trajectory shown in Figure 2. This shows the trajectory in all three dimensions. The Earth is at the origin, the Moon's orbit the grey dashed line, spacecraft trajectory the solid black line, and lunar gravitational assists are red dots.

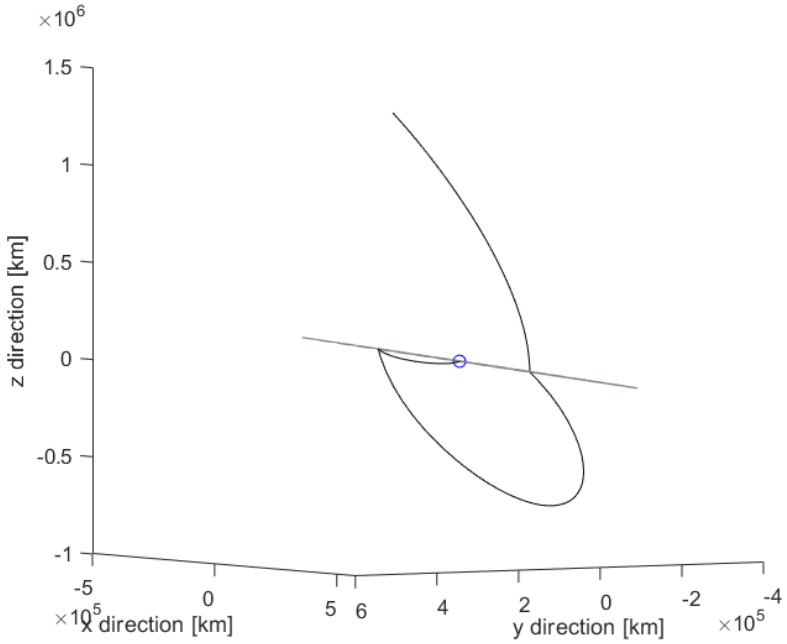

Figure 4. A different view of the trajectory shown in Figure 2. This demonstrates how each phase of the trajectory has motion out of the Earth-Moon plane. The Earth is at the origin, the Moon's orbit the grey dashed line, spacecraft trajectory the solid black line, and lunar gravitational assists are red dots.

close to the Earth, and inclination was set to 39° as this is the lowest inclination possible from a launch from Rocket Lab's New Zealand launch site. It should be noted that escape trajectories can still be found with different bounds, or no guess for any variable, as befits the mission designer.

Table 3. Results from the low-thrust Earth escape trajectory shown in Figure 2. All orbital elements here are the initial orbital elements. v_{∞_f} is final excess velocity at escape.

Parameter	Value
Launch date	14:42:45 17$^{\text{th}}$ January 2020
Argument of perigee	$-169.29°$
Eccentricity	0.967
Inclination	$39.00°$
Right ascension of ascending node	$-182.88°$
True anomaly	$0°$
v_{∞_f}	0.4048 km/s
Time of flight	64.913 days
Final mass	10.349 kg

Figures 2 shows the Earth-escape trajectory generated which uses the start conditions and produces the end results listed in Table 3. Figures 3 and 4 show the same trajectory in three dimensions to give a clearer impression of the out-of-plane motion. They show the lunar gravity assists changing the trajectory as needed to achieve escape, a result further illustrated by the plot of the magnitude of velocity over time in Figure 5. The jumps in velocity shown indicate the instantaneous change in velocity caused by the gravity assists. Figure 6 shows the change in mass over the trajectory, which steadily decreases as the spacecraft thrusts, then levels out during the coast arc. Gravity assists, like

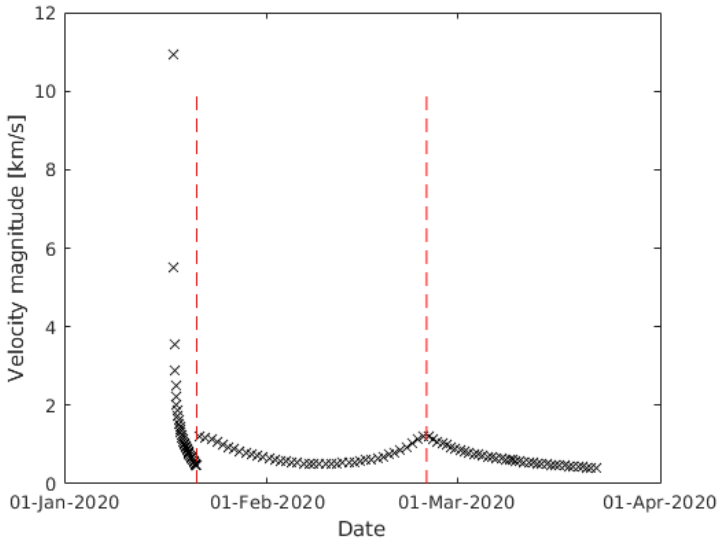

Figure 5. The magnitude of velocity over time of the trajectory in Figure 2. The discontinuities are the instantaneous changes in velocity due to lunar gravity assist. Dotted vertical red lines indicate when the gravity assists occur.

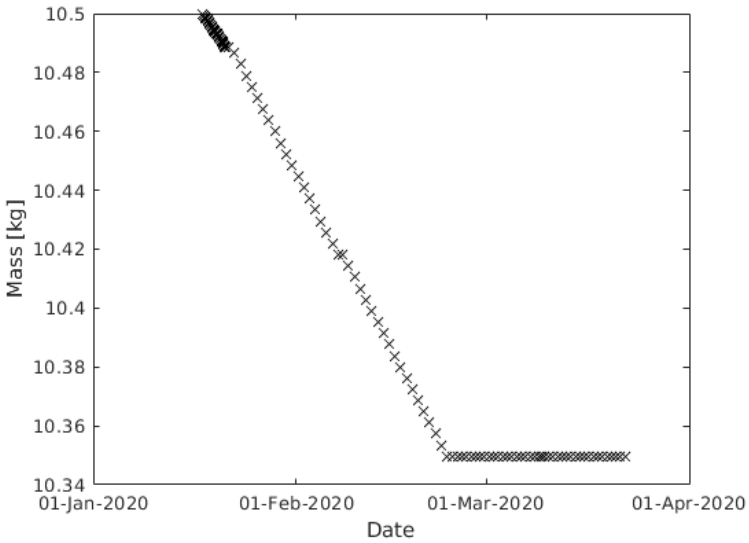

Figure 6. The mass over time of the trajectory in Figure 2.

third-body perturbations, have no effect on mass.

In previous work using MGALT, an outer loop solver has been used to autonomously decide on the flyby sequence.[15] An outer loop optimiser could be applied to this situation to eliminate a need for the mission designer to decide on the number of lunar flybys.

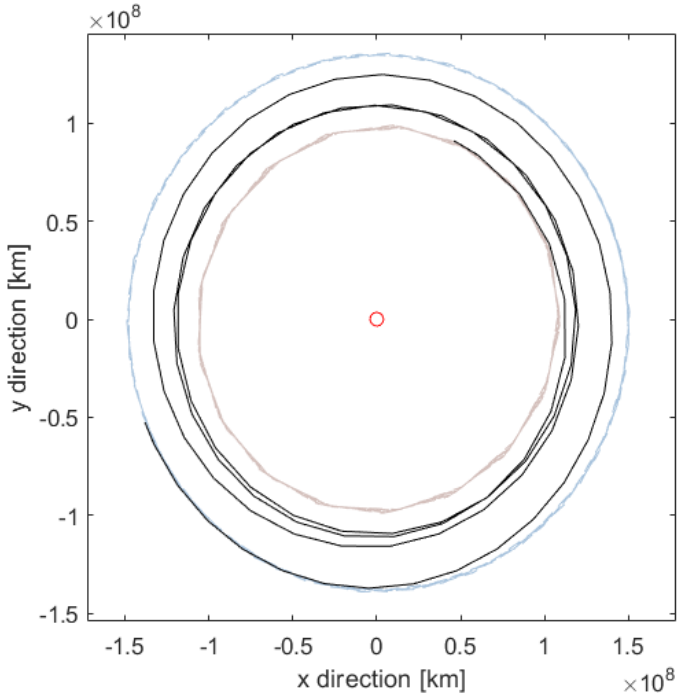

Figure 7. An Earth-Venus trajectory with starting conditions equal to the end point of the trajectory in Figure 2. The Sun is at the origin, the Earth's orbit is the blue dashed line, Venus' orbit is the brown dashed line, and the spacecraft trajectory is the solid black line.

Table 4. Results from the low-thrust Earth escape trajectory shown in Figure 7. v_{∞_f} is final excess velocity relative to Venus.

Parameter	Value
Launch date	12:37:39 22nd March 2020
Arrival date	14:38:53 05th February 2023
Time of flight	1050.1 days
v_{∞_f}	1.3890 km/s
Final mass	6.2624 kg

EARTH-VENUS TRAJECTORY

The second trajectory generated is the journey from the Earth to Venus. The initial conditions of this are set as the end conditions of the Earth-Moon escape trajectory, so that together a single continuous trajectory from injection into Earth orbit to arrival at Venus is generated. The decision variables for this trajectory are shown in Table 1. The starting conditions are fixed, rather than being decision variables, to ensure continuity. The single phase was divided into 100 segments. Launch epoch, initial mass, and velocity at Earth escape are forced to be equal to the final values from the Earth-escape trajectory. Since the interplanetary stage consists of a single phase with no gravity assist manoeuvre, no decision variables for velocity before or after gravity assist were needed, only for final velocity on arrival at Venus. Final velocity relative to Venus was constrained to be less than 1.5 km/s as higher velocities offer poorer opportunities for flybys low enough to provide much time for science missions to take place.

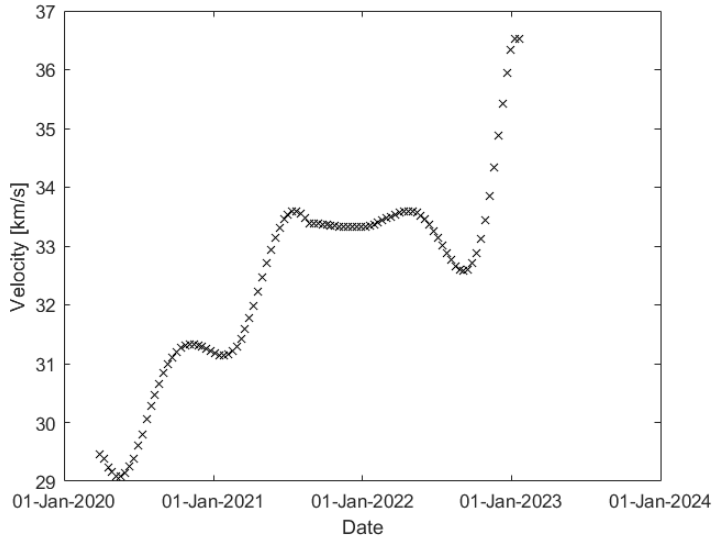

Figure 8. The magnitude of velocity over time of the trajectory in Figure 7.

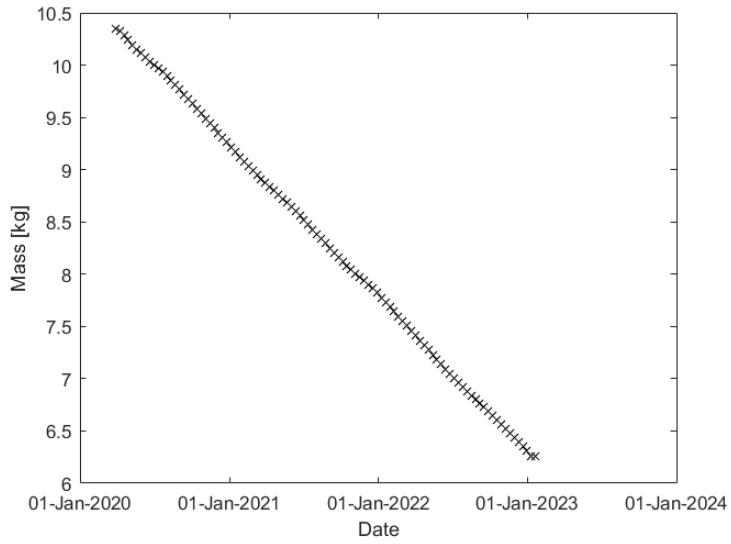

Figure 9. The mass over time of the trajectory in Figure 7.

Figure 7 shows the heliocentric Earth-Venus trajectory. The values of parameters associated with the trajectory are presented in Table 4. These show the spacecraft must make several spirals inward towards the Sun before its thrusting, modelled as continuous and always on, provides enough velocity change to meet Venus. Figure 8 shows the velocity over time. The large increase at the end is caused by closer approach with Venus, as Venus' third-body perturbations provide more acceleration closer it. Figure 9 shows the changing mass, which decreases when the thrusters are fired.

Overall, the journey from launch to arrival at Venus takes 1115 days (3.05 years) and burns 4.2376

kg of fuel. Better trajectories are possible but hindered by fixing the start conditions, so future work is possible in allowing the optimiser for the Earth-Venus trajectory to change the decision variables of Earth-escape trajectory.

There is also scope for future work in modelling arrival at Venus more rigorously. The Earth-Venus trajectory could be patched to a third Venus-centred model, with the start conditions for Venus capture or flyby equal to the final conditions of the Earth-Venus trajectory. Furthermore, an outer loop optimiser could be used to control the flyby sequence both during Earth-Moon escape to explore the effects of different numbers of lunar gravity assists, and during the Earth-Venus trajectory.

CONCLUSIONS

An automatic process for the preliminary trajectory design of low-thrust small satellites is sought after to save a mission designer having to supply a difficult, non-intuitive initial guess. Further difficulties arise as small satellites are highly unlikely to have a dedicated launch, so must be launched in rideshare missions instead of being injected directly onto a desired interplanetary trajectory. This work uses an MGALT model based off the Sims-Flanagan transcription and patched conics to develop a model capable of generating trajectories from the Earth-Moon system using lunar gravity assist manoeuvres from a launch achievable by an Electron vehicle. The results of this are patched as the start point for an Earth-Venus trajectory. Combined, the model generates a low-fidelity preliminary design for a low-thrust trajectory to Venus starting from a non-interplanetary launch from Earth, including modelling Earth escape with lunar gravity assists.

ACKNOWLEDGMENT

The authors would like to thank Ryo Nakamura for useful feedback, Bruno Sarli for helpful conversations during this project, Peter Beck and Morgan Bailey at Rocket Lab USA for providing information on the Electron vehicle, and Antonella Caldarelli for helpful discussions regarding low-thrust propulsion systems.

REFERENCES

[1] J. V. Breakwell, "The Optimization of Trajectories," *J. Soc. Indust. Appl. Math.*, Vol. 7, No. 2, 1959, pp. 215–247, 10.1137/0107018.

[2] D. J. Jezewski, "Primer Vector Theory and Applications," *Tech. Rep. TR-R454, NASA*, 1975.

[3] P. J. Enright and B. A. Conway, "Discrete approximations to optimal trajectories using direct transcription and nonlinear programming," *Journal of Guidance, Control, and Dynamics*, Vol. 15, No. 4, 1992, pp. 994–1002, 10.2514/3.20934.

[4] S. Tang and B. A. Conway, "Optimization of Low-Thrust Interplanetary Trajectories Using Collocation and Nonlinear Programming," *J. Guid. Control Dyn.*, Vol. 18, No. 3, 1995, pp. 599–604.

[5] C. H. Yam, D. Izzo, and D. D. Lorenzo, "Low-thrust trajectory design as a constrained global optimization problem," *Proceedings of the Institution of Mechanical Engineers, Part G: Journal of Aerospace Engineering*, Vol. 225, No. 11, 2011, pp. 1243–1251, 10.1177/0954410011401686.

[6] P. E. Gill, W. Murray, and M. A. Saunders, "SNOPT: An SQP algorithm for large-scale constrained optimization," *SIAM Rev.*, Vol. 47, 2005, pp. 99–131.

[7] A. E. Petropoulos, J. M. Longuski, and N. X. Vinh, "Shape-Based Analytic Representations of Low-Thrust Trajectories for Gravity-Assist Applications," *AAS/AIAA Astrodynamics Conference*, Girdwood, AK, USA, 1999, pp. 563–582.

[8] A. E. Petropoulos and J. M. Longuski, "Shape-Based Algorithm for Automated Design of Low-Thrust, Gravity-Assist Trajectories," *J. Spacecraft Rockets*, Vol. 41, No. 5, 2004, pp. 787–796, 10.2514/1.13095.

[9] E. Taheri, I. Kolmanovsky, and E. Atkins, "Shaping Low-Thrust Trajectories with Thrust-Handling Feature," *Adv. Space Res.*, Vol. 61, 2018, pp. 879–890.

[10] J. A. Sims and S. N. Flanagan, "Preliminary Design of Low-Thrust Interplanetary Missions," *AAS/AIAA Astrodynamics Specialist Conference*, Girdwood, AK, USA, August 1999.

[11] D. J. Wales and J. P. K. Doye, "Global Optimization by Basin-Hopping and the Lowest Energy Structures of Lennard-Jones Clusters Containing up to 110 Atoms," *The Journal of Physical Chemistry A*, Vol. 101, No. 28, 1997, pp. 5111–5116.

[12] M. Vasile, E. Minisci, and M. Locatelli, "Analysis of Some Global Optimization Algorithms for Space Trajectory Design," *Journal of Spacecraft and Rockets*, Vol. 47, No. 2, 2010, pp. 334–344.

[13] J. A. Englander and A. C. Englander, "Tuning Monotonic Basin Hopping," *International Symposium on Space Flight Dynamics 2014*, Vol. 24, 2014, pp. 1–33.

[14] A. Klesh, B. Clement, C. Colley, J. Essmiller, D. Forgette, J. Krajewski, A. Marinan, T. Martin-mur, J. Steinkraus, D. Sternberg, T. Werne, and B. Young, "MarCO : Early Operations of the First CubeSats to Mars," *32nd Annual AIAA/USU Conference on Small Satellites*, 2018, pp. 1–6.

[15] J. A. Englander, B. A. Conway, and T. Williams, "Automated interplanetary trajectory planning," *AIAA/AAS Astrodynamics Specialist Conference*, 2012, 10.2514/6.2012-4517.

[16] J. A. Englander, D. H. Ellison, and B. A. Conway, "Global Optimization of Low-Thrust, Multiple-Flyby Trajectories at Medium and Medium-High Fidelity," *AAS/AIAA Space Flight Mechanics Meeting*, Santa Fe, NM, 2014, pp. 1539–1558.

[17] D. H. Ellison, J. A. Englander, and B. A. Conway, "A Time-Regularized Multiple Gravity-Assist Low-Thrust Bounded-Impulse Model for Trajectory Optimization," *27th AAS/AIAA Space Flight Mechanics Meeting*, San Antonio, TX, 2017, pp. 661–674.

[18] N. Strange, D. Landau, R. Hofer, J. S. Snyder, T. Randolph, S. Campagnola, J. Szabo, and B. Pote, "Solar Electric Propulsion Gravity-Assist Tours For Jupiter Missions," *AIAA/AAS Astrodynamics Specialist Conference*, August 2012.

[19] R. H. Battin, *Introduction to the Mathematics and Methods of Astrodynamics*. American Institute for Aeronautics and Astronautics, 1999.

[20] G. J. Der, "An Elegant State Transition Matrix," *AIAA/AAS Astrodynamics Conference, San Diego, CA*, 1996, pp. 776–791, 10.2514/6.1996-3660.

[21] B. A. Conway, "An Improved Algorithm due to Laguerre for the Solution of Kepler's Equation," *Celest. Mech.*, Vol. 39, No. 2, 1986, pp. 199–211.

[22] J. A. Englander and B. A. Conway, "An Automated Solution of the Low-Thrust Interplanetary Trajectory Problem," *J. Guid. Control Dyn.*, Vol. 40, No. 1, 2017, pp. 15–27, 10.2514/1.G002124.An.

[23] C. H. Acton, "Ancillary Data Services of NASA's Navigation and Ancillary Information Facility," *Planetary and Space Science*, Vol. 44, No. 1, 1996, pp. 65–70.

[24] C. Acton, N. Bachman, B. Semenov, and E. Wright, "A look toward the future in the handling of space science mission geometry," *Planetary and Space Science*, Vol. 150, 2017, pp. 9–12.

[25] D. H. Ellison, B. A. Conway, J. A. Englander, and M. T. Ozimek, "Analytic Gradient Computation for Bounded-Impulse Trajectory Models Using Two-Sided Shooting," *J. Guid. Control Dyn.*, Vol. 41, No. 7, 2018.

[26] D. H. Ellison, B. A. Conway, J. A. Englander, and M. T. Ozimek, "Application and Analysis of Bounded-Impulse Trajectory Models with Analytic Gradients," *J. Guid. Control*, Vol. 41, No. 8, 2018.

[27] D. H. Ellison, J. A. Englander, and B. A. Conway, "Robust global optimization of low-thrust, multiple-flyby trajectories," *Advances in the Astronautical Sciences*, Vol. 150, 2014, pp. 3213–3232.